Available online at www.sciencedirect.com
ScienceDirect
Journal of Sound and Vibration 323 (2009) 17–32
JOURNAL OF SOUND AND VIBRATION
www.elsevier.com/locate/jsvi

Modelling the effect of rail dampers on wheel–rail interaction forces and rail roughness growth rates

B.E. Croft*, C.J.C. Jones, D.J. Thompson

Institute of Sound and Vibration Research, University of Southampton, Southampton SO17 1BJ, UK

Received 28 July 2008; received in revised form 20 November 2008; accepted 3 December 2008
Handling Editor: C.L. Morfey
Available online 16 January 2009

Abstract

Trains generate rolling noise because of the roughness of the wheel and rail running surfaces. Special acoustic grinding programmes have been introduced on some railways specifically to control rolling noise. Rail dampers are also used to reduce rolling noise; this paper studies rail damping as a possible mechanism to slow the rate of development of roughness on the surface of rails. This would reduce noise further over time or reduce the required frequency of grinding. High roughness growth on the rail occurs in situations with stiff vertical structural dynamics of the track. In particular the antiresonance above a sleeper at the pinned–pinned frequency has been identified as a wavelength fixing mechanism for short pitch corrugation. Rail dampers change the dynamic response of the rail, shifting the pinned–pinned frequency and smoothing the track receptance. Here, a simple time-stepping model is applied to calculate the interaction forces between wheel and rail for a track with and without rail dampers. The calculations show that rail dampers reduce dynamic interaction forces and shift the force spectrum to longer wavelengths. The interaction forces are used as input to an abrasive wear model to predict the roughness growth rate and the change in roughness after many wheel passages. Track without rail dampers is predicted to develop corrugation at the wavelength corresponding to the pinned–pinned frequency. With rail dampers the corrugation growth is reduced and shifted to a longer wavelength where its significance is diminished.
© 2008 Elsevier Ltd. All rights reserved.

1. Introduction

The dominant source of railway noise is that induced by the wheels rolling over the rails, except at very high speeds when aerodynamic noise can become the most significant source. This rolling noise has a broad spectrum in the frequency range up to about 5000 Hz, and its level and frequency content increase with train speed. The inherent roughness of the wheels and rails in the contact zone induces a relative motion which results in dynamic interaction forces, vibration of the wheels and track structures, and noise radiation. The roughness of the wheel and rail therefore has a significant effect on the noise level from a passing train. Theoretical models such as TWINS [1] exist to predict the noise resulting from a given roughness input, and

*Corresponding author. Tel.: +44 23 8059 2936; fax: +44 23 8059 3190.
E-mail address: bc1@isvr.soton.ac.uk (B.E. Croft).

0022-460X/$ - see front matter © 2008 Elsevier Ltd. All rights reserved.
doi:10.1016/j.jsv.2008.12.013

these allow different wheel and track designs to be compared. However, these models do not account for changes in roughness over time or assess the effect that a change in design may have on the propensity of the system to develop roughness. Characteristics of the system which influence the rate of roughness growth of the railhead must be assessed.

Rail damping devices have been designed in order to reduce at source the component of railway rolling noise radiated by the track [2,3]. The rail dampers proposed by Thompson et al. [2] are tuned, damped mass–spring absorber systems, with either a single mass or two masses enclosed in an elastomeric material. These rail dampers have been installed at several sites in Europe, with some variations in design. One version is continuously applied, bonded along each side of each rail, with a narrow rail damper footprint providing clearance for the rail fastening system. A more recent design, as tested in the Silence project [4], utilises discrete clipped-on rail dampers, attached to the rail in pairs in the middle of each sleeper bay. The rail dampers affect the dynamic response of the track structure to the time-varying wheel–rail interaction, reducing the effective radiating length of the rail by increasing the track decay rate [5]. Measurements in the Silent Track project with soft rail pads and a low noise wheel have shown a reduction in overall noise of 5.6 dB, with a reduction in the track noise component of over 6 dB [2].

Although it is known that rail damping reduces rolling noise [6], the resulting change in the track dynamics may also affect the roughness growth rate in the longer term. Moreover, the occasions of rail 'corrugation' damage that also lead to a strong increase in the noise may be avoided or controlled where it is found to occur. Here 'corrugation' is defined as the rapid development of a strong periodic component in the otherwise broadband spectrum of roughness. Corrugation has several forms and causes [7], of interest in this work is the short pitch corrugation that has been linked to the pinned–pinned antiresonance of the track.

The first step towards predicting the change in roughness of the railhead over time is to develop a model of the track and vehicle. This is used to calculate the response of the track to the excitation arising from the movement of the wheels over the combined roughness of the surfaces. The resulting dynamic normal interaction forces between the wheels and the rail may be input into a model of the stresses in the contact patch with a wear calculation to predict the resulting change in the railhead roughness profile after many wheel passages.

In 1993 Knothe and Grassie [8] completed a comprehensive review of the modelling of railway track and vehicle/track interaction for frequencies up to 5000 Hz. Most interaction force models may be categorised as either time domain or frequency domain models. Frequency domain models are necessarily linear, whereas time domain models may include nonlinearities. Historically, time domain models have required a large computational capacity, whereas frequency domain models are usually more efficient, albeit less flexible. It is common to assume either a nonlinear or linearised Hertzian contact spring at the wheel–rail interface in order to calculate the overall force in the wheel–rail contact. Knothe and Grassie consider this Hertzian approach to be adequate for the calculation of the vertical interaction forces provided the filtering effect of the discrete size of the contact patch on the forces is taken into account [8].

The size of the contact patch and the distribution of normal and tangential stresses at each point in time are then predicted from the overall vertical force. In 2001 Knothe et al. [9] reviewed the state of the art in techniques for modelling wheel–rail contact mechanics. Kalker's three-dimensional variational method as described in Ref. [10] and implemented in the program CONTACT is considered the most encompassing model available, including both non-Hertzian and non-steady effects. 'Non-steady' means the tangential stress distribution in the contact is calculated progressively at each location, dependent on the solution for the previous location. The main limitation of CONTACT is the computation time, as in order to deal with micro-roughness of the surface, an extremely fine discretisation is required. Alternatively the simplest contact models proposed for the prediction of rail roughness growth assume Hertzian contact and neglect lateral forces and creepages, focussing on longitudinal creepage [11–13]. In general, contact models may be divided into Hertzian (which assumes smooth surfaces) or non-Hertzian, and either steady or non-steady. Recent work by Xie and Iwnicki [14] has shown that different conclusions on roughness growth may be drawn depending on the type of contact model used.

Commonly, frictional abrasive wear is assumed as the mechanism for roughness growth [11–13,15]. The amount of material removed is taken to be proportional to the work done by the tangential stress in the slip zone of the contact patch. Alternative wear mechanisms such as plastic deformation [16] and ratchetting

wear [17] have been proposed, and it is likely that multiple wear mechanisms exist, or that different wear mechanisms dominate at different sites.

Despite the uncertainty over the mechanism of roughness growth, the wavelength fixing mechanism of short pitch corrugations is well understood [18]. It is generally accepted that the wavelength of short pitch corrugations is determined by resonances in the coupled train–track system, in particular the pinned–pinned resonance of the rail, which is a bending mode of the rail with the sleepers giving rise to nodes and the sleeper spacing corresponding to half a wavelength. Other vertical antiresonances in the track and system resonances between the two wheelsets of a bogie can also fix the wavelength of corrugation [19,20]. Hempelmann and Knothe [15] developed a linear model for the prediction of short pitch corrugation, obtaining an exponential growth law for corrugation formation. They compared frequency-dependent corrugation growth rates at certain positions in a sleeper bay with the track receptance. Their results predict higher corrugation growth rates in situations with stiff vertical structural dynamics of the track. This occurs where the rail has a strong antiresonance such as above the sleepers at the pinned–pinned frequency.

Both Hiensch et al. [12] and Nielsen [11] have suggested remedying high roughness growth by increasing the track receptance above the sleepers at the pinned–pinned frequency, by adding damping to the rails. The idea is to smooth the minima in the track receptance and hence achieve lower interaction forces. The present work demonstrates that rail dampers developed to control noise radiation from the track also have an effect on the track dynamics, resulting in reduced interaction forces and hence in reduced roughness or corrugation growth. The work has been carried out in parallel with measurement tests at a site in southern Germany (Gersthofen) as part of the EU project 'Silence'.

2. Wheel–track interaction force model

For this work a two-dimensional time domain model has been used to determine the vertical wheel–rail interaction forces. A simple two dimensional non-steady Hertzian model is used to determine the size of the contact patch and the normal and tangential stress distribution in the contact. The mechanism for roughness growth is assumed to be frictional abrasive wear. While these choices involve some simplification, the purpose of the present work is to study the relative propensity of a plain line track to develop roughness with and without rail dampers.

2.1. Finite element model of track and vehicle

A finite element model of 50 sleeper bays of UIC60 track has been set up as shown in Fig. 1. This model is based on that developed by Nielsen et al. [11,21]. The rail model includes four Timoshenko beam elements per sleeper bay. Half the track only is considered, i.e. a single rail on half-sleepers. Track parameters are chosen to

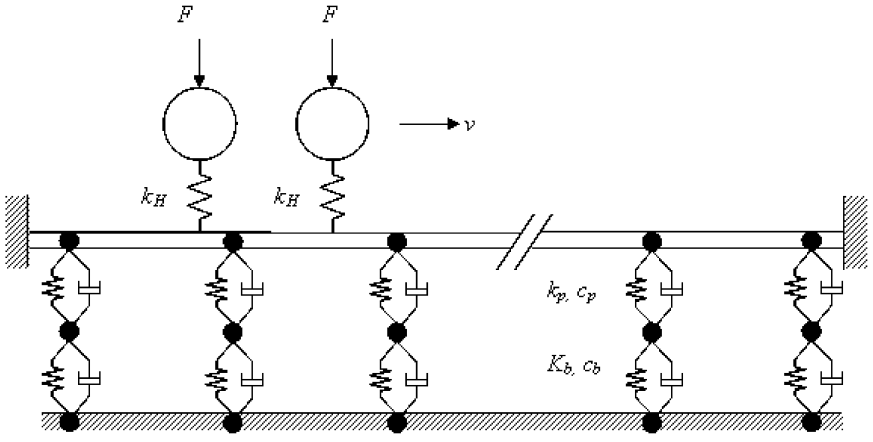

Fig. 1. Representation of track and vehicle system.

Table 1
Train parameters.

Parameter	Freight train	Regional train	ICE train
Vehicle velocity	$29.44\,\mathrm{m\,s^{-1}}$	$37.78\,\mathrm{m\,s^{-1}}$	$43.06\,\mathrm{m\,s^{-1}}$
Unsprung wheel mass	488.5 kg	702.5 kg	782 kg
Static load on wheel	$100\times10^3\,\mathrm{N}$	$60\times10^3\,\mathrm{N}$	$60\times10^3\,\mathrm{N}$
Wheel spacing	1.8 m	2.5 m	2.5 m

match the Silence project test site. The half-sleepers are modelled as 147 kg masses equally spaced at 0.6 m intervals, while rail pads and ballast are modelled as spring–damper sets. Two rail pad stiffnesses k_p of 2×10^8 and $8\times10^8\,\mathrm{N\,m^{-1}}$ are considered in order to model tracks with soft and stiff pads, respectively. The rail pad damping c_p is $5\times10^3\,\mathrm{N\,s\,m^{-1}}$, the ballast stiffness k_b is $5\times10^7\,\mathrm{N\,m^{-1}}$ and the ballast damping c_b $1\times10^5\,\mathrm{N\,s\,m^{-1}}$. The track ends are constrained in displacement and rotation. The degrees of freedom of the model allow displacement in the vertical direction and rotation in the vertical plane. Lateral effects are not included. The vehicle is modelled by two uncoupled wheel masses moving at velocity v, each linked to the rail by a Hertzian contact spring k_H of stiffness $1.4\times10^9\,\mathrm{N\,m^{-1}}$. An external static force F represents the sprung vehicle mass. The wheelbase and wheel loads vary with each train type and are listed in Table 1.

2.2. Inclusion of rail dampers

Addition of rail dampers is achieved by adding additional elements to the finite element model in each sleeper bay. The dampers are represented by three models of increasing complexity as shown in Fig. 2. To represent the properties of the elastomeric material, a combination of Maxwell elements in parallel with a spring is used as shown.

The simplest damper model consists of a single lumped mass (Fig. 2a). This arrangement results in a damper tuning frequency of 1050 Hz which is very close to the pinned–pinned frequency of the track. The impedance of this lumped mass model of the rail dampers in isolation is shown in Fig. 3. A more realistic representation of an actual damper design is as a beam attached at two points in each sleeper bay (Fig. 2b). The final damper model is a continuous beam attached at all the nodes along the rail (Fig. 2c). The damper installed at the Silence test site is similar to the second of these models, but with two beams and two tuning frequencies.

Implementing Maxwell elements in a finite element code results in a singularity in the absence of any mass at the node between each spring and damping element. To circumvent this difficulty, small additional masses (with natural frequencies well above the range of interest) are included at each of the intermediate nodes. For example the single lumped mass model of the damper (Fig. 2a) includes two masses of 0.2 kg each giving a natural frequency of 5780 Hz. Proportionally smaller masses are used in the other damper designs depending on the number of Maxwell elements.

The equations of motion of the damper elastomer element as shown in Fig. 4 (neglecting the small masses for simplicity) are

$$\begin{bmatrix} c_{d1}+c_{d2} & -c_{d1} & -c_{d2} \\ -c_{d1} & c_{d1} & 0 \\ -c_{d2} & 0 & c_{d2} \end{bmatrix} \begin{bmatrix} \dot{x}_1 \\ \dot{x}_2 \\ \dot{x}_3 \end{bmatrix} + \begin{bmatrix} k_d & 0 & 0 \\ 0 & k_{d1} & 0 \\ 0 & 0 & k_{d2} \end{bmatrix} \begin{bmatrix} x_1 \\ x_2 \\ x_3 \end{bmatrix} = \begin{bmatrix} f_1 \\ 0 \\ 0 \end{bmatrix} \tag{1}$$

These equations of motion may be rearranged to eliminate the internal degrees of freedom x_2 and x_3, resulting in an equation of the form $f=kx$, where k is the complex, frequency-dependent stiffness of the elastomer:

$$f_1 = \left(\frac{c_{d1}^2\omega^2}{c_{d1}\mathrm{i}\omega + k_{d1}} + \frac{c_{d2}^2\omega^2}{c_{d2}\mathrm{i}\omega + k_{d2}} + c_{d1}\mathrm{i}\omega + c_{d2}\mathrm{i}\omega + k_d \right) x_1 \tag{2}$$

For ideal hysteretic damping $f=k(1+\mathrm{i}\eta)x$ where η is the loss factor. The imaginary part of the bracketed term in Eq. (2) may be normalised by dividing by the stiffness of the spring k_d and compared with the nominal design loss factor of the rubber of 0.34.

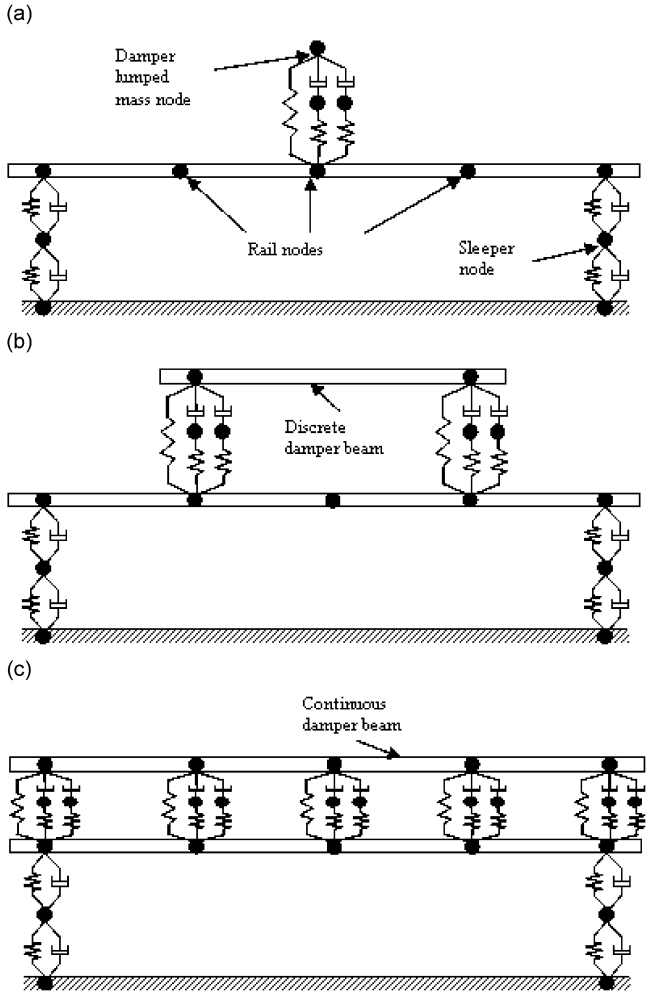

Fig. 2. Representation of a rail dampers: (a) a single lumped mass on spring and damper elements, (b) a discrete beam attached to the rail at two points in each sleeper bay, (c) a continuous beam attached to the rail at each rail node.

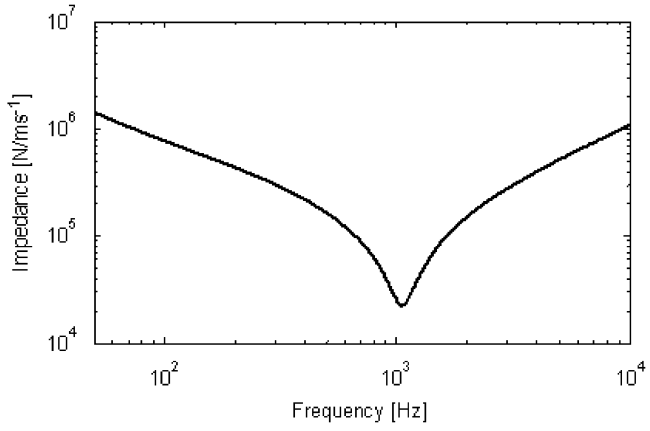

Fig. 3. Impedance of rail damper modelled as a lumped mass as in Fig. 2a.

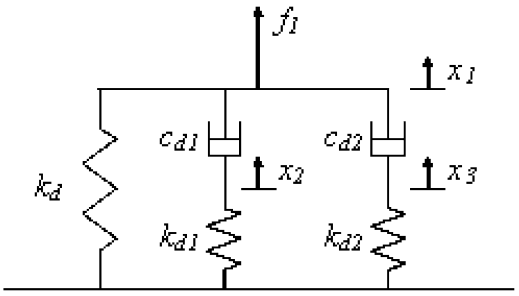

Fig. 4. Degrees of freedom of damper rubber element (neglecting masses).

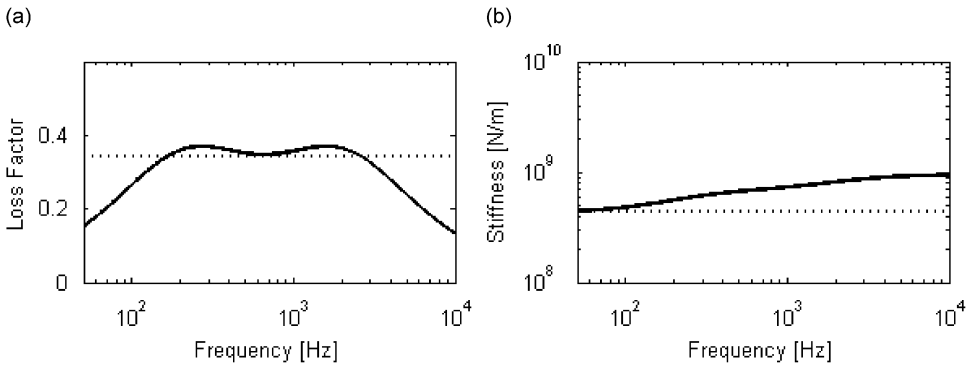

Fig. 5. Equivalent frequency-dependent loss factor and stiffness of finite element model of rail dampers tuned to a natural frequency of 800 Hz: (a) loss factor, (b) stiffness. —— as modelled; ····· nominal value.

The equivalent frequency-dependent loss factor and stiffness of the rail damper elastomer modelled in this way are shown in Fig. 5. In practice the stiffness of the elastomer used in rail dampers increases significantly with frequency, consequently the model can be made (as here) a better representation of the elastomer stiffness than would be achieved using a single frequency-independent value. By combining two Maxwell elements in parallel a loss factor roughly constant over the frequency range from 100 to 3000 Hz is achieved while an increase in stiffness with frequency of a factor of approximately two occurs in the same range.

2.3. Finite element modal analysis

Global mass, stiffness and damping matrices for the track are assembled and the modes of vibration of the system are calculated using standard finite element methods. The frequency range of interest is limited so, to reduce calculation times, only modes with natural frequencies up to 3000 Hz are included. The track receptance over a sleeper is calculated from a modal analysis based on the finite element model and is shown in Fig. 6 for the track with and without rail dampers. The finite element model parameters were tuned to those of the test site by comparing calculated decay rates [5] with measured track decay rates.

For track without rail dampers, the pinned–pinned antiresonance in the receptance above a sleeper occurs at just over 1000 Hz. This feature is stronger for the track with stiffer rail pads. The addition of rail dampers to the system in all cases shifts the pinned–pinned antiresonance to a lower frequency. The depth of the antiresonance is also reduced. The single mass and discrete beam damper models have a similar effect on the receptance, although the discrete beam damper model introduces an additional antiresonance to the system just below 2000 Hz. The continuous damper beam model, while still shifting the pinned–pinned frequency, also introduces further relatively small peaks and troughs into the receptance in the frequency range above 800 Hz.

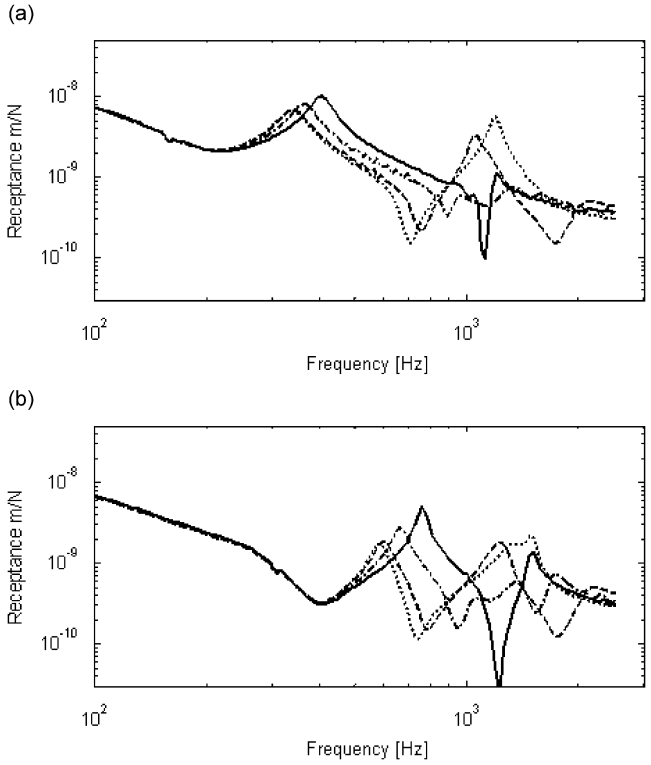

Fig. 6. Predicted track vertical receptance above a sleeper with and without the addition of rail dampers: (a) track with soft rail pads, (b) track with stiff rail pads. —— without rail dampers; ····· lumped mass rail dampers; – – – discrete beam rail dampers; – · – · continuous beam rail dampers.

The changes in receptance are due to the additional mass of the discrete rail dampers, and also the additional resonances of the track system in particular with the continuous beam damper model.

3. Wheel–track interaction force results

The modal forms of the equations of motion for the track, vehicle and their interaction are solved as a state space system using a standard time-stepping routine with variable step size in similar fashion to the technique used by Nielsen and Igeland [21]. An initial low-level roughness profile has been generated from a sum of 30 sine functions in each one-third octave wavelength band, with random phase, to match the measured roughness spectrum. This roughness is filtered using the method described in Ref. [22] to take account of the filtering effect of the contact patch. The interaction forces between the wheels and the rail are determined as the wheels move along the model of the track in the time domain.

The traffic at the Gersthofen test site is mixed. Three train types are modelled here as separate cases: freight, regional and ICE trains, using typical parameters for each as in Table 1. The wheel radius of all vehicles is 0.46 m.

The interaction force spectrum for each case has been calculated from the time history of the force over the middle 10 sleeper bays of the model, for each of the two wheels in the vehicle. Results are shown for the first wheel only, although small differences are found between the two wheels. Figs. 7 and 8 show the effect of the dampers on the interaction force. The forces are plotted as a function of wavelength rather than frequency to allow easier comparison with the predictions of roughness growth. Due to the long calculation times involved, the analysis of the discrete beam and continuous damper designs is completed for the freight train only. For the freight vehicle on track with both soft and stiff rail pads the predicted interaction force

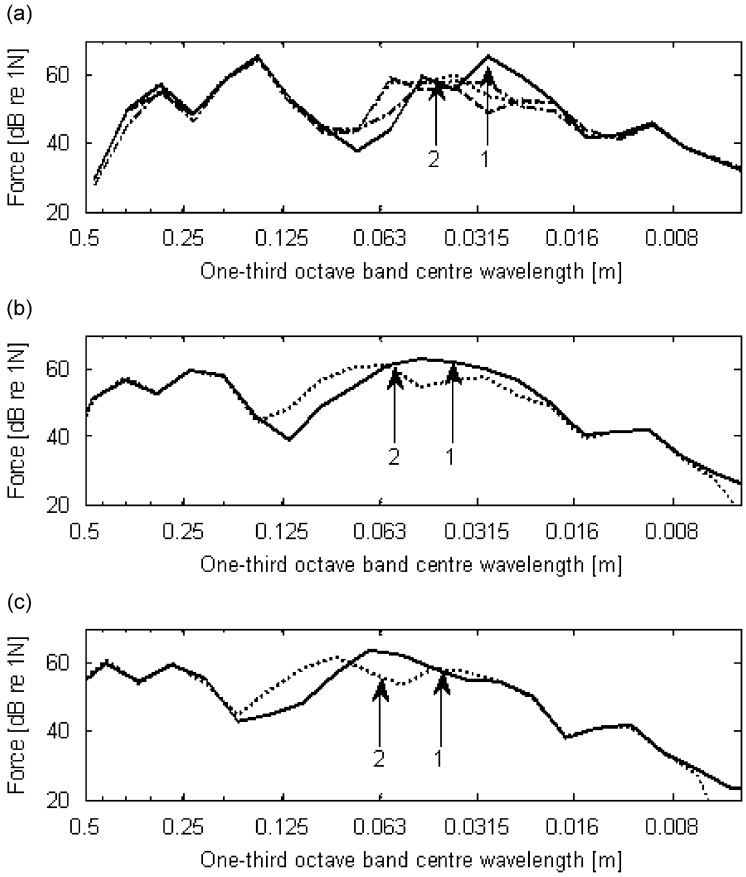

Fig. 7. Predicted wheel–track dynamic vertical interaction force with and without the addition of rail dampers on track with soft pads: (a) typical freight train, (b) typical regional train, (c) typical ICE train. —— without rail dampers; ····· lumped mass rail dampers; – – – discrete beam rail dampers; – · – · continuous beam rail dampers. Numbered arrows indicate wavelength corresponding to pinned–pinned frequency: 1 without rail dampers; 2 with rail dampers.

spectra are similar for all three damper designs, so the results are not heavily dependent on the details of the damper design. Similar results are also achieved if the damper tuning frequency is varied in the range from 500 to 1100 Hz.

Different wavelengths are dominant for each of the train types due to their differing average speeds and wheel spacings. The shift in the force spectrum to longer wavelengths when the dampers are applied corresponds to the shift in the pinned–pinned frequency observed in the track receptance (Fig. 6). In each case, the dynamic interaction force in the one-third octave wavelength band corresponding to the original pinned–pinned frequency without rail dampers is reduced. The effect on the pinned–pinned frequency is bigger with the stiff rail pads than with the soft rail pads. A reduction in the peak dynamic interaction force of 2–3 dB is observed for all train types although this peak does not necessarily occur at the pinned–pinned wavelength. For all cases the interaction forces at short wavelengths are low, due to the filtering effect of the contact patch.

4. Wear model

The wear has also been calculated over the middle 10 sleeper bays of the model. The force at each wheel as they pass over these sleeper bays has been extracted from the results of the time-stepping calculation and used in conjunction with the initial rail profile in those sleeper bays to predict the wear of the rail after a large number of wheel passages. Wear is assumed to be proportional to the work done by the tangential stress q in the slip zone of the contact patch, so that the change in the rail profile $\Delta z(x)$ after a single wheel passages is

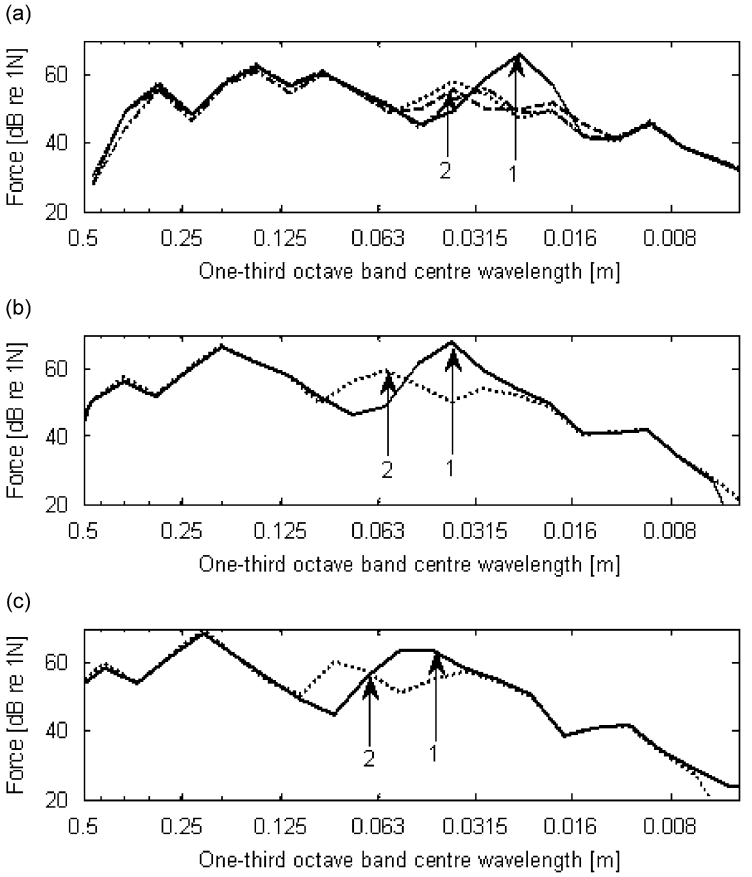

Fig. 8. Predicted wheel–track dynamic vertical interaction force with and without the addition of rail dampers on track with stiff pads: (a) typical freight train, (b) typical regional train, (c) typical ICE train. —— without rail dampers; ····· lumped mass rail dampers; – – – discrete beam rail dampers; – · – · continuous beam rail dampers. Numbered arrows indicate wavelength corresponding to pinned–pinned frequency: 1 without rail dampers; 2 with rail dampers.

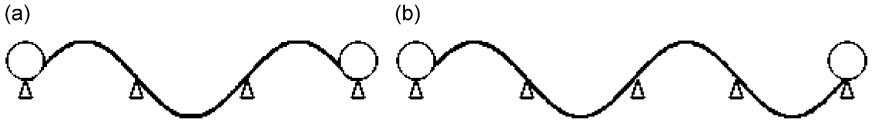

Fig. 9. Pinned–pinned bending mode of discretely supported rail between two wheels of bogie: (a) freight wheel spacing 1.8 m (b) regional and ICE wheel spacing 2.5 m.

given by Sheng et al. [13] as

$$\Delta z(x) = \frac{1}{\rho}\int_{t_1}^{t_2} K|q(x,t)s(x,t)|\,\mathrm{d}t \tag{3}$$

where ρ is the density of the rail, s is the slip velocity, t_1 and t_2 are the times at which the position x along the rail enters and leaves the contact area. K is the wear constant, taken to be 2.5×10^{-9} kg/N m in this case as in Ref. [11].

The wear model is two dimensional as in Ref. [13], simplifying the contact patch to a rectangle of constant width. The longitudinal creepage, i.e. the relative velocity of the wheel and rail expressed as a percentage of the rolling velocity, is assumed to be constant with a value of 0.1%. There is no variation in forces or roughness

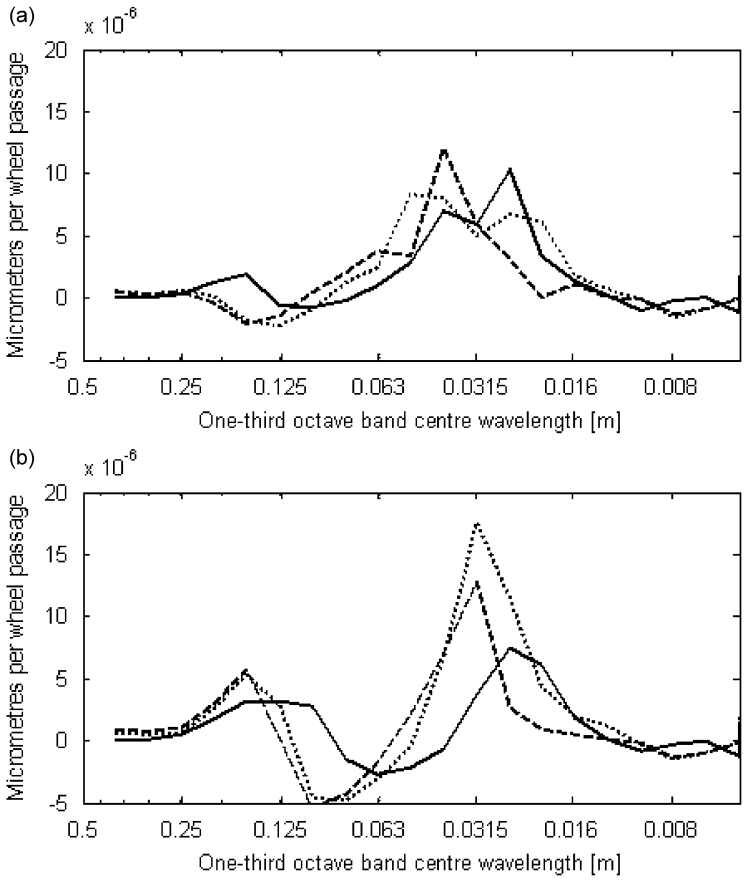

Fig. 10. Predicted roughness growth rate spectrum for track without rail dampers for each vehicle: (a) soft rail pads, (b) stiff rail pads. —— freight; ····· regional; – – – ICE.

growth across the railhead. In each time interval the length of the Hertzian contact patch is determined from the vertical interaction force at that point. This contact patch is divided into a stick zone and a slip zone as in Ref. [13]. The frictional work and hence the wear are calculated in the slip zone, and this wear accumulates over many wheel passages to form a revised rail profile.

In a situation with broadband roughness including components of wavelength shorter than the contact length, it is necessary to neglect the curvature of the roughness profile at each point when calculating the contact patch length, that is the rail is considered smooth for this part of the calculation. Including the curvature in this situation would result in multiple contact points which are not addressed by the assumption of Hertzian contact conditions. The curvature should be considered if a corrugation wavelength greater than the length of the contact patch is present. The contact may only be approximated using Hertz theory for low roughness amplitudes.

For the purposes of this study the results are presented as a global roughness growth rate which is independent of the number of wheel passages (and the initial roughness level). The concept of a 'global growth rate' is described in Ref. [15]. It allows the comparison of results for roughness or corrugation predictions that are calculated for different input parameters and different reference states. A global growth rate is a single spectrum providing a mean value for the prediction in each one-third octave wavelength band for the full length of track included in the investigation. The global growth rate γ is calculated from the initial roughness amplitude A_0 and the final roughness amplitude A_n in each wavelength band k after n wheel passages as

$$\gamma_k = \frac{1}{n}\ln\left(\frac{A_{k,n}}{A_{k,0}}\right) \tag{4}$$

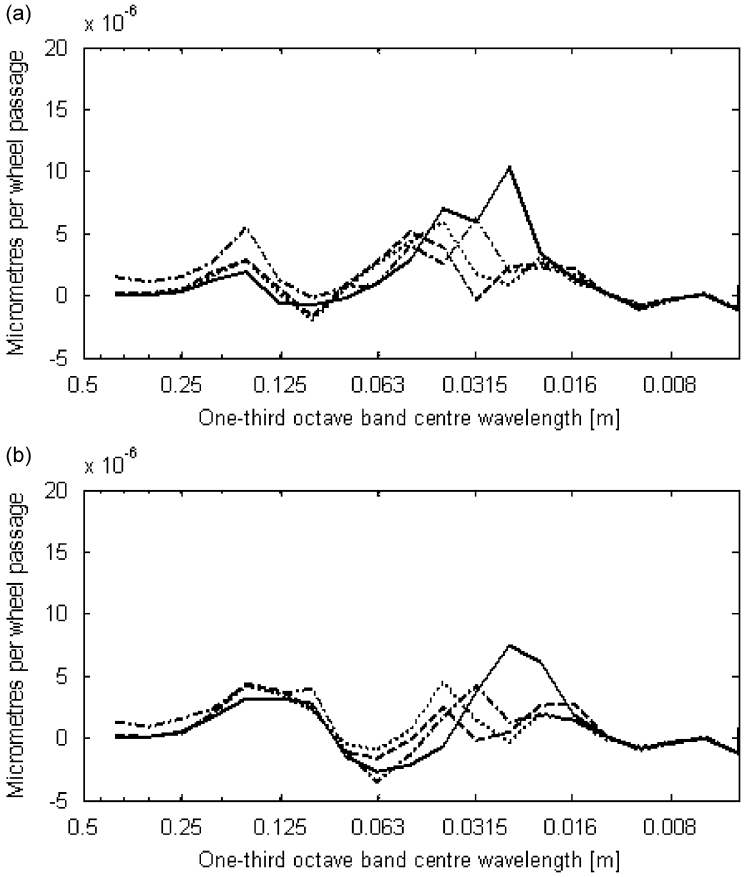

Fig. 11. Predicted roughness growth rate spectrum from typical freight train with the addition of rail dampers compared to the roughness developed for an undamped track: (a) soft rail pads, (b) stiff rail pads. —— original roughness growth rate; ⋯⋯ roughness growth rate with lumped mass damper model; – – – roughness growth rate discrete beam damper model; – · – · roughness growth rate with continuous beam damper model.

It is an important aspect of the model that two wheels have been included running on the same rail. This allows for wave reflections along the rail between the successive wheels in a bogie, which has been shown to be a possible corrugation wavelength fixing mechanism in addition to the pinned–pinned mode [19]. For the freight vehicle, the wheel spacing of 1.8 m happens to be exactly three sleeper bays. The roughness wavelength corresponding to a standing wave between these two wheels (and also corresponding to the pinned–pinned mode, shown in Fig. 9a) is 0.026 m. The regional and ICE vehicle wheel spacing of 2.5 m is close to four sleeper bays, with corresponding standing wavelengths and pinned–pinned wavelengths of 0.034 m for the regional vehicle and 0.042 m for the ICE vehicle. Other standing waves can also occur between successive wheels, as the rail may vibrate with different numbers of half-wavelengths between the two wheels, see Ref. [19].

5. Predicted rail roughness growth rates

Fig. 10 shows the roughness growth rates for track without rail dampers, for the three vehicle types considered. Note that for the track with stiff pads the peak roughness growth rates are generally higher (except for the freight case), supporting the overall theory that stiffer rail pads lead to higher roughness and corrugation growth rates. However, the roughness growth rates do not correspond exactly to the pinned–pinned antiresonances in the receptance, as if they did there would be a clear progression in the peaks to longer wavelengths with increasing vehicle speed. Further work investigating continuously and

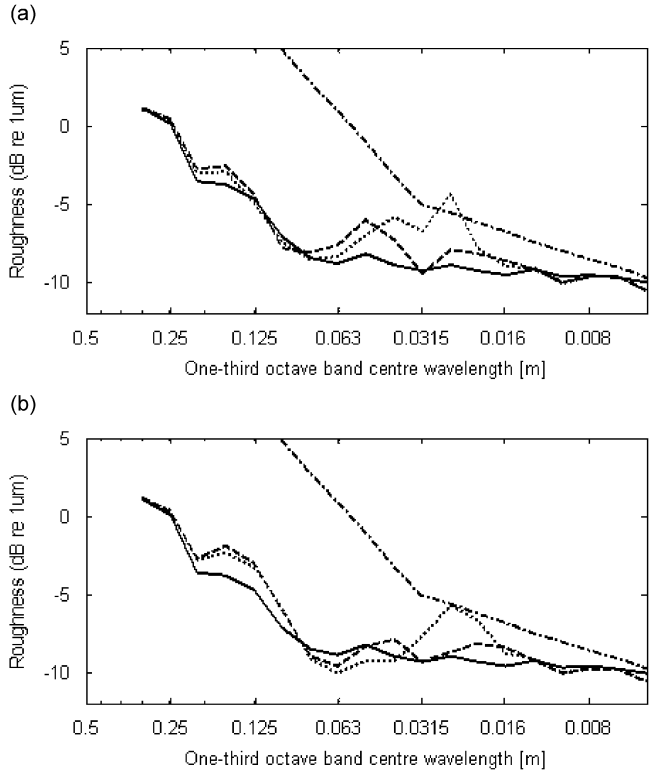

Fig. 12. Predicted roughness spectrum from typical freight train with the addition of rail dampers compared to the roughness developed for an undamped track: (a) soft rail pads, (b) stiff rail pads. —— initial roughness level; ····· final roughness level without rail dampers; – – – final roughness level with rail dampers (discrete beam model); – · – · TSI+ limit spectrum.

discretely supported track is required to understand the relative importance of the bogie wheel spacing compared to the pinned–pinned resonance.

Adding rail dampers to the track reduces the roughness growth rates for all damper designs considered as shown in Fig. 11. Due to long interaction force calculation times when the rail dampers are included in the model, this analysis has been completed for freight trains only. The different rail damper designs result in slightly different roughness growth rates, but no damper design gives significant benefits over the others in reducing the roughness growth rate.

The roughness growth rate plots do not present the growth in the context of the initial roughness spectrum. Therefore, although the wear constant that has been used is somewhat arbitrary, Fig. 12 shows the roughness spectrum predicted to develop after 2×10^5 wheel passages of purely freight traffic at the site, without rail dampers and with the discrete beam damper model. As the wear from a single wheel passage is very small it is assumed that any resulting change in interaction forces is also very small. The wear after the passage of the two wheels in the model may then be multiplied to simulate thousands of wheel passages, without recalculating the contact forces [11]. In this work a factor of 1×10^5 is used to simulate wear over 2×10^5 wheel passages in a single iteration of the wear model. Fig. 13 gives an example of the predicted change in the roughness profile in one sleeper bay after this many wheel passages.

The initial roughness level is very low. As a reference, the spectral limit stated in the technical specifications for interoperability (TSIs) is also shown in Fig. 12 [23]. The model predicts that after 2×10^5 wheel passages without rail dampers, roughness will grow significantly at wavelengths between 0.016 and 0.063 m on track with soft pads, and at wavelengths between 0.0125 and 0.04 m on track with stiff pads. The peak roughness growth for both tracks is predicted to occur in the 0.025 m wavelength one-third octave band, corresponding to the pinned–pinned frequency for the freight vehicle speed. Shorter wavelengths are not expected to grow. Significant roughness growth at longer wavelengths is not indicated by the model.

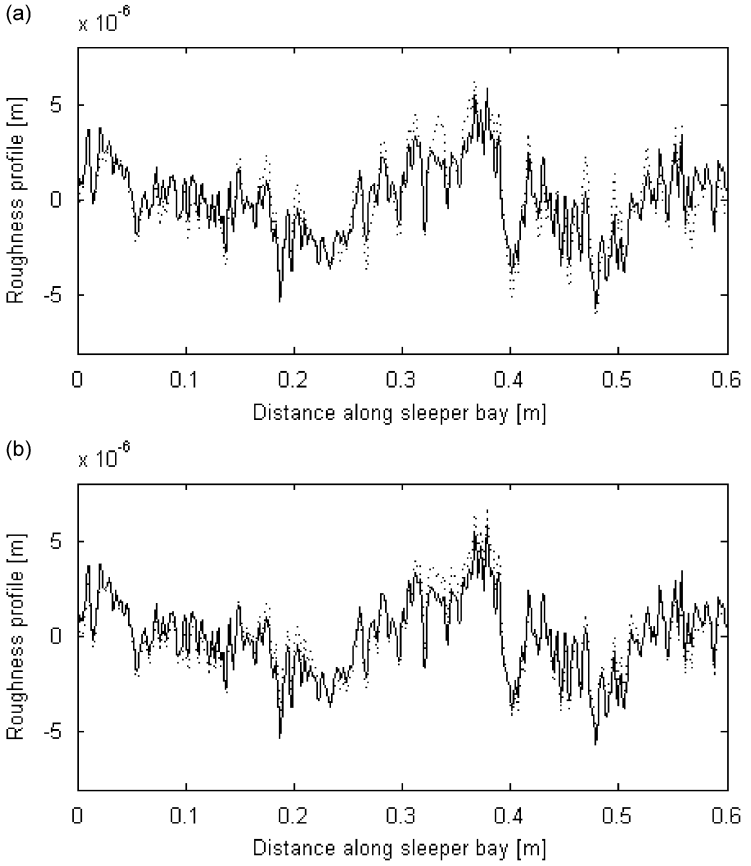

Fig. 13. Predicted change in roughness profile in a single sleeper bay after 2×10^5 wheel passages of typical freight traffic on track with soft rail pads: (a) without rail dampers, (b) with rail dampers (discrete beam model). —— initial roughness profile; ⋯⋯ final roughness profile.

With the rail dampers applied, the peak predicted roughness level and roughness growth rate displays a shift to longer wavelengths reflecting the shift in the pinned–pinned frequency. At the original pinned–pinned frequency of the track, the roughness is not predicted to grow significantly with the rail dampers applied. The predicted peak roughness level is also reduced by the inclusion of the rail dampers in the model.

At the Silence project test site the traffic is made up of a mixture of different train types. Around 44% of the total wheel passages are due to freight, 22% are due to regional traffic and the remaining 34% are due to high-speed ICE traffic. The wear of the track as a result of mixed traffic has been estimated by adding the change in the rail profile due to each train type multiplied by the corresponding percentage. The resulting roughness growth rates for mixed traffic are shown in Fig. 14 and the corresponding predicted roughness spectra in Fig. 15, for the same total number of wheel passages as used previously. In both these figures the rail damper model is the single lumped mass type. The combined roughness growth rate per wheel passage for mixed traffic is lower than the roughness growth rates for particular train types shown in Fig. 10. There is less difference in the results for mixed traffic and individual trains for track with rail dampers. The effect of the rail dampers to reduce roughness growth at some wavelengths is therefore slightly less when the traffic is mixed compared to when a single train type is modelled, for the same number of wheel passages.

6. Conclusions

Rail dampers are shown to shift the pinned–pinned frequency of the track and to smooth the peaks and troughs in the track receptance. For each of the three rail damper cases considered, this work predicts a

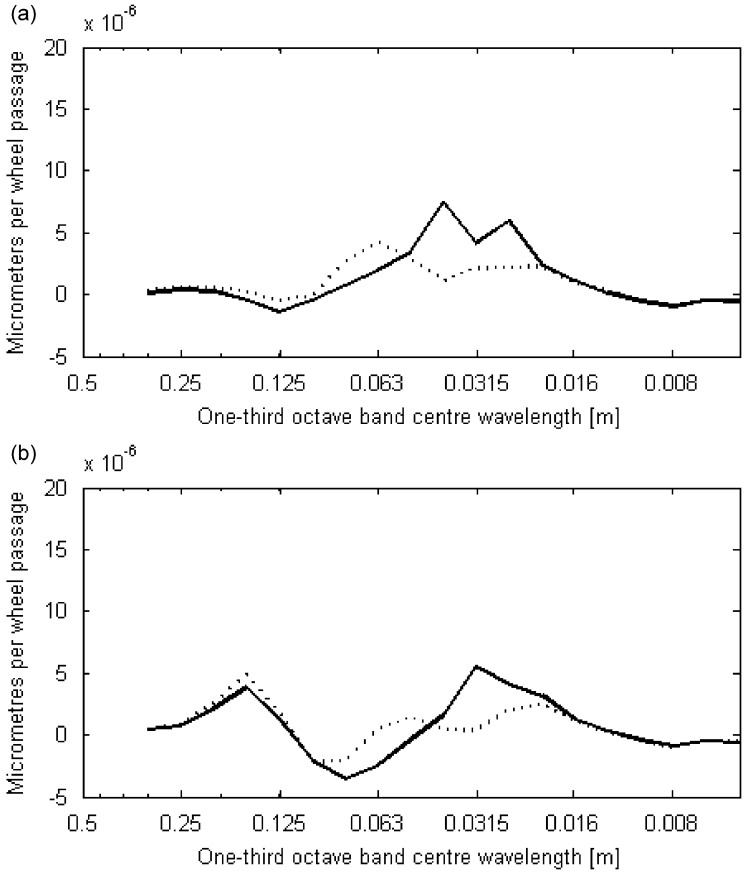

Fig. 14. Predicted roughness growth rate spectrum for mixed traffic with the addition of rail dampers compared to the roughness developed for an undamped track: (a) soft rail pads, (b) stiff rail pads. —— original roughness growth rate; ····· roughness growth rate lumped mass damper model.

decrease in interaction forces, especially around the pinned–pinned frequency, and a shift in the interaction force spectrum to lower frequencies.

The resulting roughness growth rate predicted after many wheel passages using the model of vertical dynamics of straight track supports the theory that corrugation wavelength is fixed by the pinned–pinned frequency and also by track resonances between successive wheels. The model suggests that a reduction in roughness growth compared to initial levels may be achieved by the application of rail dampers. Corresponding to the shift in the pinned–pinned frequency, any corrugation development is predicted to be reduced and shifted to a longer wavelength. The designs of rail dampers selected for this study do not form a systematic study but it can be seen that a favourable outcome is indicated for each of the cases for which results are presented here.

With this model, roughness is predicted to grow at particular wavelengths for particular train types and speeds. This would lead to corrugation (i.e. periodic wear) after many wheel passages. In practice a mixture of traffic types and speeds is in operation at this site, this mixture of traffic is expected to reduce the overall roughness growth rates.

Due to the long time required for changes in roughness to develop, it is difficult to confirm this work experimentally. Measurements of rail roughness at yearly intervals on track with and without rail dampers at the Silence project test site are ongoing and it is hoped that these measurements will provide confirmation of this work in future years.

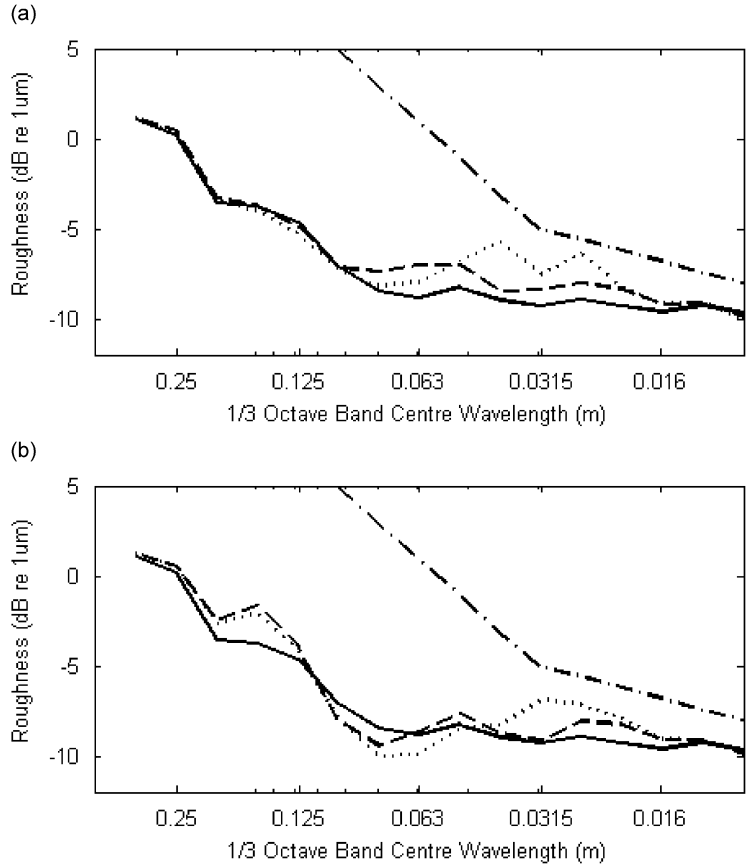

Fig. 15. Predicted roughness spectrum for mixed traffic with the addition of rail dampers compared to the roughness developed for an undamped track: (a) soft rail pads, (b) stiff rail pads. —— initial roughness level; · · · · · · final roughness level without rail dampers; – – – final roughness level with rail dampers (lumped mass model); – · – · TSI+ limit spectrum.

Acknowledgements

This work has been undertaken as part of the EU project 'Silence' (DG Research Contract no. 516 288 of FP6). The authors appreciate the assistance provided by Deutsche Bahn AG DB Systemtechnik and Corus Rail.

References

[1] D.J. Thompson, B. Hemsworth, N. Vincent, Experimental validation of the twins prediction program for rolling noise, Part 1: description of the model and method, *Journal of Sound and Vibration* 193 (1996) 123–135.

[2] D.J. Thompson, C.J.C. Jones, T.P. Waters, D. Farrington, A tuned damping device for reducing noise from railway track, *Applied Acoustics* 68 (2007) 43–57.

[3] J. Maes, H. Sol, A double tuned rail damper—increased damping at the two first pinned–pinned frequencies, *Journal of Sound and Vibration* 267 (2003) 721–737.

[4] B. Asmussen, D. Stiebel, P. Kitson, D. Farrington, D. Benton, Reducing the noise emission by increasing the damping of the rail: results of a field test. *Notes on Numerical Fluid Mechanics and Multidisciplinary Design 99. Noise and Vibration Mitigation for Rail Transportation Systems* (2008) 229–235.

[5] C.J.C. Jones, D.J. Thompson, R.J. Diehl, The use of decay rates to analyse the performance of railway track in rolling noise generation, *Journal of Sound and Vibration* 293 (2006) 485–495.

[6] D.J. Thompson, P.-E. Gautier, Review of research into wheel/rail rolling noise reduction, *Proceedings of the Institution of Mechanical Engineers, Part F: Journal of Rail and Rapid Transit* 220 (2006) 385–408.

[7] S.L. Grassie, J. Kalousek, Rail corrugation: characteristics, causes and treatments, *Proceedings of the Institution of Mechanical Engineers, Part F: Journal of Rail and Rapid Transit* 207 (1993) 57–68.
[8] K. Knothe, S.L. Grassie, Modelling of railway track and vehicle/track interaction at high frequencies, *Vehicle System Dynamics* 22 (1993) 209–262.
[9] K. Knothe, R. Wille, B.W. Zastrau, Advanced contact mechanics—road and rail, *Vehicle System Dynamics* 35 (2001) 361–407.
[10] J.J. Kalker, Three-dimensional elastic bodies in rolling contact, *Solid Mechanics and its Applications*. Vol. 2, Kluwer Academic Publishers, Dordrecht, 1990.
[11] J.C.O. Nielsen, Numerical prediction of rail roughness growth on tangent railway tracks, *Journal of Sound and Vibration* 267 (2003) 537–548.
[12] M. Hiensch, J.C.O. Nielsen, E. Verheijen, Rail corrugation in the Netherlands—measurements and simulations, *Wear* 253 (2002) 140–149.
[13] X. Sheng, D.J. Thompson, C.J.C. Jones, G. Xie, S.D. Iwnicki, P. Allen, S.S. Hsu, Simulations of roughness initiation and growth on railway rails, *Journal of Sound and Vibration* 293 (2006) 819–829.
[14] G. Xie, S.D. Iwnicki, Calculation of wear on a corrugated rail using a three-dimensional contact model, in: *7th International Conference on Contact Mechanics and Wear of Rail/Wheel Systems*, Brisbane, Australia, 2006.
[15] K. Hempelmann, K. Knothe, An extended linear model for the prediction of short pitch corrugation, *Wear* 191 (1996) 161–169.
[16] A. Bohmer, T. Klimpel, Plastic deformation of corrugated rails—a numerical approach using material data of rail steel, *Wear* 253 (2002) 150–161.
[17] F.J. Franklin, T. Chung, A. Kapoor, Ratcheting and fatigue-led wear in rail—wheel contact, *Fatigue and Fracture of Engineering Materials and Structures* 26 (2003) 949–955.
[18] S.L. Grassie, Rail corrugation: advances in measurement, understanding and treatment, *Wear* 258 (2005) 1224–1234.
[19] A. Igeland, Railhead corrugation growth explained by dynamic interaction between track and bogie wheelsets, *Proceedings of the Institution of Mechanical Engineers, Part F: Journal of Rail and Rapid Transit* 210 (1996) 11–20.
[20] T.X. Wu, D.J. Thompson, An investigation into rail corrugation due to micro-slip under multiple wheel/rail interactions, *Wear* 258 (2005) 1115–1125.
[21] J.C.O. Nielsen, A. Igeland, Vertical dynamic interaction between train and track—influence of wheel and track imperfections, *Journal of Sound and Vibration* 187 (1995) 825–839.
[22] R.A.J. Ford, D.J. Thompson, Simplified contact filters in wheel/rail noise prediction, *Journal of Sound and Vibration* 293 (2006) 807–818.
[23] BS EN ISO 3095:2005 Railway applications. Acoustics. Measurement of noise emitted by railbound vehicles.